ION CHANNELS

A pharmacological master key mechanism that unlocks the selectivity filter gate in K^+ channels

Marcus Schewe[1]*†, Han Sun[2]*, Ümit Mert[1], Alexandra Mackenzie[3,4,5], Ashley C. W. Pike[3], Friederike Schulz[1], Cristina Constantin[6,7], Kirsty S. Vowinkel[8], Linus J. Conrad[4,5], Aytug K. Kiper[8], Wendy Gonzalez[9,10], Marianne Musinszki[1], Marie Tegtmeier[1], David C. Pryde[11]‡, Hassane Belabed[12], Marc Nazare[12], Bert L. de Groot[13], Niels Decher[8], Bernd Fakler[6,7], Elisabeth P. Carpenter[3,4], Stephen J. Tucker[4,5], Thomas Baukrowitz[1]†

Potassium (K^+) channels have been evolutionarily tuned for activation by diverse biological stimuli, and pharmacological activation is thought to target these specific gating mechanisms. Here we report a class of negatively charged activators (NCAs) that bypass the specific mechanisms but act as master keys to open K^+ channels gated at their selectivity filter (SF), including many two-pore domain K^+ (K_{2P}) channels, voltage-gated hERG (human ether-à-go-go–related gene) channels and calcium (Ca^{2+})–activated big-conductance potassium (BK)–type channels. Functional analysis, x-ray crystallography, and molecular dynamics simulations revealed that the NCAs bind to similar sites below the SF, increase pore and SF K^+ occupancy, and open the filter gate. These results uncover an unrecognized polypharmacology among K^+ channel activators and highlight a filter gating machinery that is conserved across different families of K^+ channels with implications for rational drug design.

Dampening cellular electrical activity by pharmacological activation of specific types of K^+ channels has therapeutic potential for the treatment of a variety of disease states, including epilepsy, arrhythmias, vascular constriction, and various pain conditions (*1*, *2*). Consequently, screening efforts have identified a number of agents that open different types of K^+ channels (*2*), presumably by targeting their respective channel-specific activation mechanisms.

Distinct structural mechanisms enable K^+ channels to respond to a plethora of physiological stimuli, including voltage, temperature, mechanical force, and various second messengers, such as adenosine triphosphate (ATP), Ca^{2+}, and H^+, as well as bioactive lipids such as phosphatidylinositol 4,5-bisphosphate (PIP_2) and arachidonic acid (*3*, *4*). However, despite this complexity, these activation pathways seem to converge on the two principal mechanisms known to gate K^+ channels open: dilation of the "lower" gate at the intracellular pore entrance used by inwardly rectifying (K_{ir}) (*5*) and voltage-gated (K_v) K^+ channels (*6*), and activation of the selectivity filter (SF) gate used by most two-pore domain K^+ (K_{2P}) channels (*4*, *7*, *8*) and Ca^{2+}-activated big-conductance K^+ (BK_{Ca}) channels (*9*, *10*). In voltage-gated hERG (human ether-à-go-go–related gene) channels, both mechanisms coexist, with voltage opening the lower gate but rapid inactivation occurring through closure of the SF gate (*11*, *12*). Here we identify a common mechanism for drug-induced channel opening that bypasses these physiological activation mechanisms in SF-gated K^+ channels.

For the mechanosensitive K_{2P} channels TREK-1 and TREK-2, the voltage-gated hERG channel, and the Ca^{2+}-activated BK_{Ca} channel, a series of small-molecule activators all harboring a negatively charged group (tetrazole or carboxylate) have been proposed to act as selective channel openers [i.e., BL-1249 for TREK-1/-2 (*13*); PD-118057 for hERG (*14*); and NS11021 for BK_{Ca} (*15*)]. However, application of these compounds to their respective "nontarget" channels revealed an unexpected polypharmacology: All three openers displayed equal efficiency in opening TREK-1 channels (Fig. 1A) and hERG channels (Fig. 1B), as well as BK_{Ca} channels (Fig. 1C), whose activation curve is strongly shifted to more negative voltages (fig. S1C). This suggests that these activators may not target channel-specific activation mechanisms and may instead share a common mechanism. In all cases, the compound-mediated effect was effectively antagonized by large quaternary ammonium ions (QA_L^+) such as tetra-pentylammonium (TPenA) or tetra-hexyl-ammonium (THexA) that are known to block K^+ channels at a site immediately below the inner entrance to the SF (*16*) (Fig. 1, A and B, and fig. S1C). Likewise, all these activators reduced the QA_L^+-mediated inhibition in these different K^+ channels (Fig. 1C and figs. S1, A and B, and S7, A and B). Furthermore, extended screening with BL-1249 also revealed potent activation of several other K_{2P} channels (TREK-2, TRAAK, TALK-1, TALK-2, THIK-1, and THIK-2; fig. S1D). Together, these data suggest that these negatively charged activators (NCAs) (BL-1249, PD-118057, and NS11021) act on a gating mechanism that is shared among these different classes of K^+ channels and that their action involves a site that overlaps with the conserved QA_L^+-binding site located below the SF.

A distinctive feature of all NCA-responsive K^+ channels is their gating by the SF, a mechanism that is intimately coupled to ion permeation (*17*, *18*). In K_{2P} channels, this coupling leads to pronounced activation by Rb^+, which displays an ion occupancy distinct to K^+ at the four SF K^+ binding sites (S1 to S4) that stabilizes the activated state of the SF gate (*17*). Interestingly, Rb^+ not only activated all NCA-responsive K_{2P} channels but also led to robust activation of BK_{Ca} and hERG channels (Fig. 1D). By contrast, Rb^+ failed to exert any activatory effect on K^+ channels gated at the helix-bundle crossing (i.e., K_{ir} and most K_v channels), as was observed for $K_v1.1$, $K_v1.5$, $K_v3.1$, and $K_{ir}1.1$ (Fig. 1D); consistent with this, these channels were also not activated by BL-1249 (fig. S2, A to E). Furthermore, cyclic nucleotide–gated channels that are also gated at the SF were not activated by BL-1249, indicating that the NCA mechanism may be specific to SF-gated K^+ channels (fig. S2F).

To gain further mechanistic insight into channel opening by the NCAs, we next investigated their binding by x-ray crystallography, cysteine-scanning mutagenesis, and atomistic molecular dynamics (MD) simulations. First, anomalous diffraction data were collected from TREK-2 channels cocrystallized with a brominated derivative of BL-1249 ($BL\text{-}1249^{Br}$) (Fig. 2A; fig. S3, A to C; and supplementary materials and methods). Although no discrete electron density was visible for BL-1249 itself, in anomalous difference maps, two bromine peaks were clearly visible per TREK-2 dimer (fig. S3, A and B) and the main-chain protein backbone showed excellent agreement with a previously crystallized high-resolution structure of TREK-2 [Protein Data Bank (PDB) 4XDJ] (*19*). Both bromine anomalous difference peaks were located at the entrance of the side fenestrations branching off the central pore cavity below the SF. Comparison with a structure

[1]Institute of Physiology, Christian-Albrechts University of Kiel, 24118 Kiel, Germany. [2]Leibniz-Forschungsinstitut für Molekulare Pharmakologie (FMP), Department of Structural Biology, 13125 Berlin, Germany. [3]Structural Genomics Consortium, University of Oxford, Oxford OX3 7DQ, UK. [4]OXION Initiative in Ion Channels and Disease, University of Oxford, Oxford OX1 3PN, UK. [5]Clarendon Laboratory, Department of Physics, University of Oxford, Oxford OX1 3PU, UK. [6]Institute of Physiology II, Albert-Ludwigs University of Freiburg, 79104 Freiburg, Germany. [7]Centers for Biological Signaling Studies CIBSS and BIOSS, 79104 Freiburg, Germany. [8]Institute of Physiology and Pathophysiology, Vegetative Physiology, Philipps-University of Marburg, 35037 Marburg, Germany. [9]Centro de Bioinformatica y Simulacion Molecular, Universidad de Talca, 3465548 Talca, Chile. [10]Millennium Nucleus of Ion Channels-Associated Diseases (MiNICAD), Universidad de Talca, 3465548 Talca, Chile. [11]Pfizer Worldwide Medicinal Chemistry, Neuroscience and Pain Research Unit, Portway Building, Granta Park, Great Abington, Cambridgeshire CB21 6GS, UK. [12]Leibniz-Forschungsinstitut für Molekulare Pharmakologie (FMP), Department of Medicinal Chemistry, 13125 Berlin, Germany. [13]Computational Biomolecular Dynamics Group, Max Planck Institute for Biophysical Chemistry, 37077 Göttingen, Germany.
*These authors contributed equally to this work.
†Corresponding author. Email: m.schewe@physiologie.uni-kiel.de (M.S.); t.baukrowitz@physiologie.uni-kiel.de (T.B.) ‡Present address: Curadev Pharma Ltd., Sandwich Kent, UK.

that included QA_L^+ (*16*) showed that these bromine positions reside within the spherical volume of THexA but outside that of the smaller tetra-ethyl-ammonium (TEA) ion. Consistent with this, BL-1249 activation of TREK-2 channels was antagonized by THexA but not by TEA (Fig. 2, B and C).

These structural data were complemented by cysteine-scanning mutagenesis of the pore-lining M2 and M4 helices of TREK-1. Six residues, including the highly conserved Pro^{183} (P183) and Leu^{304} (L304) (also investigated in TREK-2, fig. S3D), were identified where mutations markedly reduced the apparent affinity of BL-1249. These residues cluster around the bromine densities

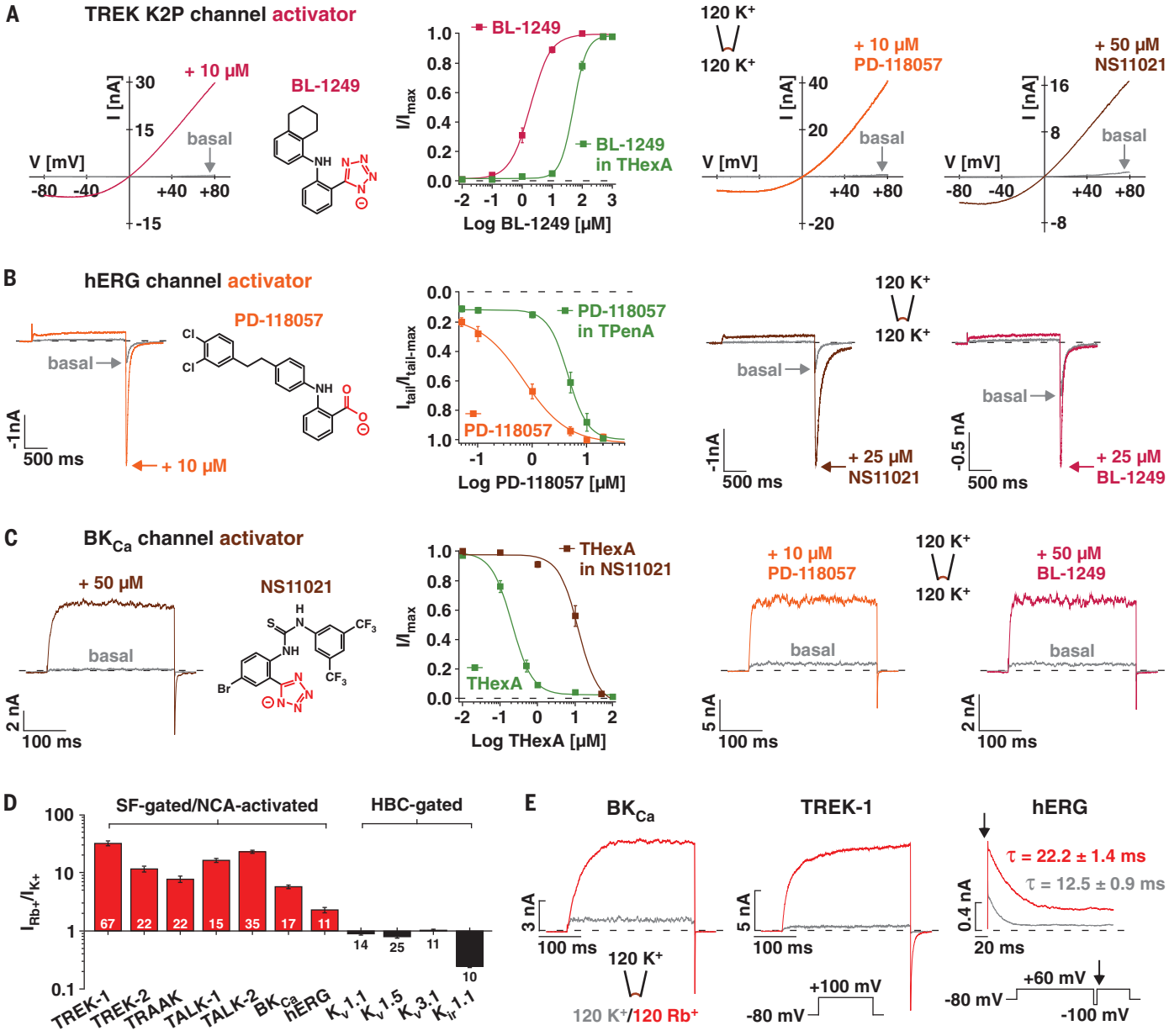

Fig. 1. NCAs open SF-gated K^+ channels via a similar site.
(**A**) Representative TREK-1 channel currents recorded in inside-out (i-o) patches evoked by voltage ramps in the absence (basal) and presence of the indicated compounds. BL-1249 (compound structure shown) dose-response curves represent currents at +40 mV and with or without 5 µM THexA that produced 77 ± 6% inhibition of basal currents ($n \geq 8$). I, current; V, voltage. (**B**) hERG channel currents (voltage steps from −80 to +60 mV) in i-o patches with or without the indicated compounds; arrows indicate peak tail current amplitudes at −100 mV. PD-118057 (compound structure shown) dose-response curves represent normalized tail currents with or without 1 µM TPenA that produced 91 ± 1% inhibition of basal currents ($n \geq 6$). (**C**) BK_{Ca} channel currents [voltage steps from a holding potential of −80 to +100 mV (zero Ca^{2+})] in i-o patches with or without the indicated compounds. THexA inhibition represents currents at +100 mV and with or without 50 µM NS11021 (compound structure shown; $n \geq 11$). (**D**) Rb^+ effects on different K^+ channels measured in i-o patches. Bars ± SEM represent fold change of outward currents upon exchange of intracellular K^+ by Rb^+ for K_{2P} and BK_{Ca} channels (+100 mV); for hERG, $K_v1.1$, $K_v1.5$, and $K_v3.1$ channels (+60 mV); and for $K_{ir}1.1$ channels (+40 mV). The channels are grouped as either SF-gated and NCA-activated or helix-bundle crossing (HBC)–gated. (**E**) Representative traces of Rb^+ activation for BK_{Ca}, TREK-1, and hERG channels using the indicated protocols [arrow indicates the starting point of hERG inactivation after inactivation recovery (at −100 mV)]. Time constant (τ) values from monoexponential fits to inactivation time course ($n \geq 12$). For (A) to (C), errors bars indicate SEM.

detected in the TREK-2 cocrystal with BL-1249^{Br} (Fig. 2D and fig. S3, C and D). A role for L304 in this presumed binding site was further supported by cysteine-modification protection experiments in which the time course of irreversible pore blockade induced by application of the cysteine-modifying agent MTS-TBAO [8-(tributylammonium)octyl methanethiosulfonate] (*20*) to TREK-1 L304C (Leu^{304}→Cys) channels was markedly slowed by the presence of BL-1249 (Fig. 2, E and F). This effect was specific for BL-1249, as two further channel activators with distinct binding sites [2-APB at the C terminus (*21*) and ML335 behind the SF (*22*)] both failed to slow this rate (Fig. 2, E and F). Furthermore, TREK-1 activation with 2-APB or ML335 was not antagonized by QA_L^+ inhibition, and mutations at the BL-1249 site did not affect 2-APB activation (fig. S4, A, B, and E).

In addition, we performed MD simulations to examine the orientation of BL-1249^{Br} within its proposed binding site (Fig. 2G). The favored binding pose oriented the negatively charged tetrazole group of BL-1249 toward the S6 "cavity binding site" for K^+ just below the SF. The remainder of the BL-1249 molecule engaged with residues in M2 and M4 consistent with our scanning mutagenesis data (Fig. 2D and fig. S3D). Moreover, the bromine atom in these simulations was found to be within 3 to 4 Å of the bromine densities determined by crystallography (fig. S3E). Together, these data indicate that BL-1249 binds to a site below the SF and reveal a critical role of the negative charge of the acidic tetrazole ring (pK_a around 5, where K_a is the dissociation constant), implying a pH-dependent compound efficacy. Indeed, when tested with the K_{2P} channel TALK-2 [exhibiting little intrinsic intracellular pH (pH$_i$) sensitivity], BL-1249 potency dropped strongly with a lowering of the solution pH$_i$ to 5, whereas control experiments with 2-APB lacked this pH dependence (Fig. 3F).

We have recently used atomistic MD simulations and a double-bilayer setup to study ion permeation in the TRAAK K_{2P} channel (*17*). Therefore, we carried out simulations of ion permeation in

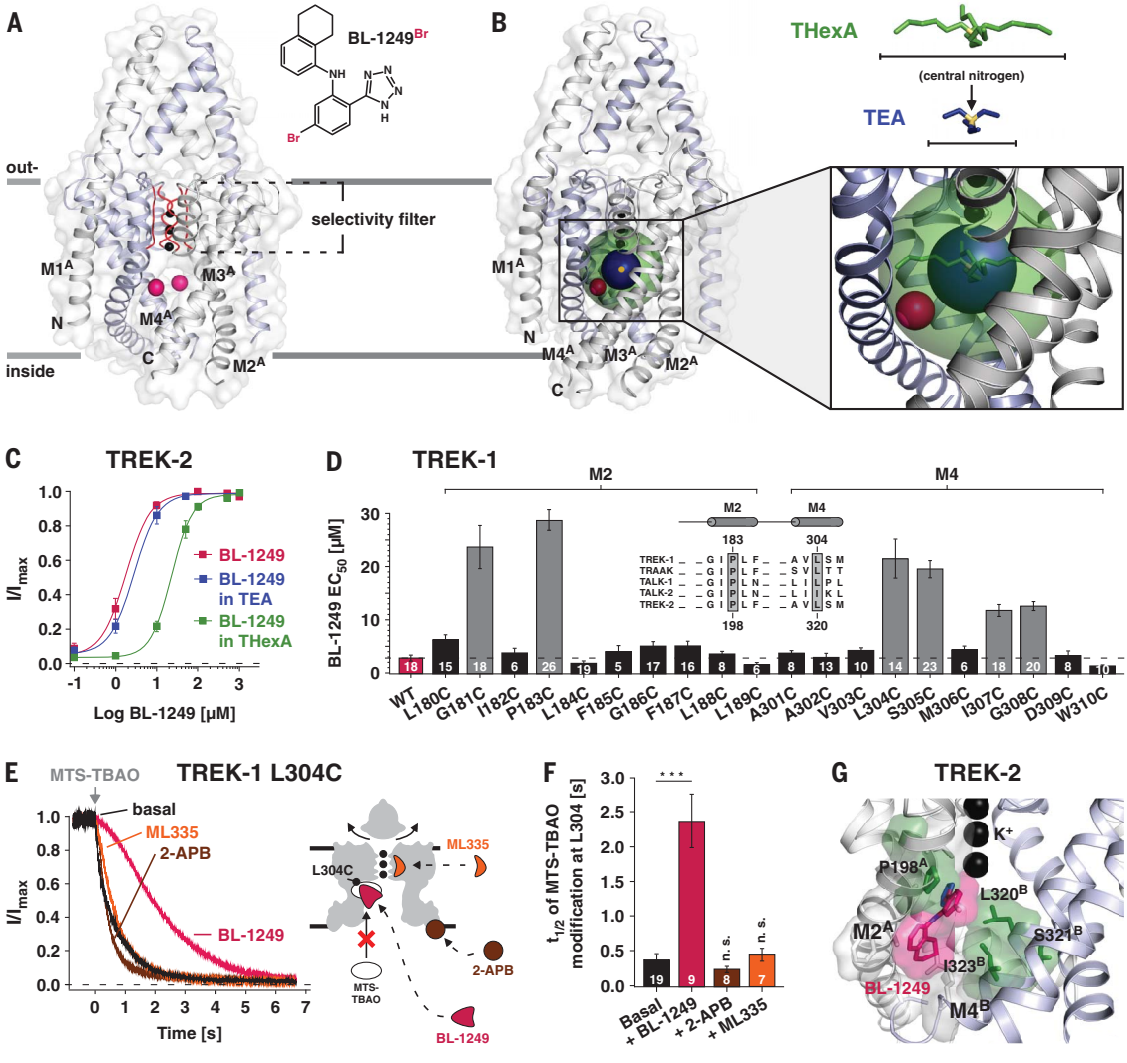

Fig. 2. Identification of the BL-1249 binding site in TREK K_{2P} channels. (**A**) The structure depicts TREK-2 (PDB 4XDJ), with pink spheres representing the positions of Br atoms in a brominated BL-1249 derivate (BL-1249Br) obtained by cocrystallization of TREK-2 and BL-1249Br (see also fig. S3). With this medium-resolution data, only the Br atoms were identified, because they gave peaks in anomalous difference maps. N, N terminus; C, C terminus. (**B**) The same structure also showing spherical representations of THexA (green) and TEA (dark blue) with their central nitrogen atoms (yellow). Their positions are based on the crystal structures of KcsA with QA^+s (*16*). Note that the Br atoms [pink spheres in (A)] are within the sphere of THexA but not of TEA. (**C**) BL-1249 dose-response curves for TREK-2 with or without 100 mM TEA ($n \geq 12$) or 5 μM THexA ($n \geq 13$) (TEA and THexA produce 74 ± 3 and 83 ± 2% basal current inhibition, respectively). Error bars indicate SEM. (**D**) Scanning mutagenesis of M2 and M4 helices showing BL-1249 median effective concentration (EC_{50}) values ± SEM determined at +40 mV; the inset shows a K_{2P} channel alignment for channels strongly activated by BL-1249 (see also fig. S1D) with residues homologous to TREK-1 P183 and L304 highlighted. (**E**) Time courses of 10 μM MTS-TBAO cysteine modification of L304C in TREK-1 before and after maximal activation by BL-1249 (50 μM), ML335 (50 μM), and 2-APB (1 mM) (left panel). The graphic depicts TREK-1 with predicted drug binding sites relative to the position of residue L304C. (**F**) Time values ± SEM for half-maximal MTS-TBAO modification inhibition ($t_{1/2}$) in the presence of different agonists. ***$P \leq 0.001$; n.s., not significant. (**G**) Representation of favored binding pose of BL-1249 (pink) in TREK-2 along with the location of the TREK-1 corresponding mutations (green) that reduce BL-1249 activation. For (A) and (G), the A and B superscripts indicate the subunit of the TREK-2 dimer. Single-letter abbreviations for amino acid residues are as follows: A, Ala; C, Cys; D, Asp; E, Glu; F, Phe; G, Gly; H, His; I, Ile; K, Lys; L, Leu; M, Met; N, Asn; P, Pro; Q, Gln; R, Arg; S, Ser; T, Thr; V, Val; W, Trp; and Y, Tyr.

TRAAK with BL-1249 modeled into the equivalent site in the TRAAK channel structure (PDB 4I9W) (Fig. 3A). This indicated several changes induced by BL-1249: (i) K^+ occupancy at the S6 site located adjacent to the negatively charged tetrazole group of BL-1249 increased ~16-fold (Fig. 3, A and B), (ii) K^+ occupancy of the S1 and S4 sites increased (Fig. 3B), and (iii) the rate of K^+ permeation increased by 1.6-fold (24 ± 2 ions/μs compared to 15 ± 2 ions/μs without BL-1249; Fig. 3C).

The effect of BL-1249 on ion permeation was further investigated with single-channel recordings of TREK-2 expressed in human embryonic kidney (HEK) 293 cells. Besides an increase in open probability, an increase in the measured single-channel amplitude was also observed in both the inward (from −29.3 ± 1.5 to −34.1 ± 1.9 pA at −100 mV; n = 7) and outward (from 17.7 ± 1.3 to 21.7 ± 1.4 pA at +100 mV; n = 7) directions in response to BL-1249 (Fig. 3, D and E). This result is consistent with the observed increase in SF ion occupancy at S1 and S4 that is expected to enhance ion permeation via a direct knock-on effect for ions entering the SF from either side (*23*). A similar increase in unitary conductance was also observed for TREK-1 channels recorded in patches from *Xenopus* oocytes (fig. S4, A to C). Notably, increases in single-channel conductance have not been observed upon activation of TREK-1, TREK-2, or TRAAK K_{2P} channels by other physiological stimuli (*24*, *25*).

Collectively, these results indicate that BL-1249 increases ion permeation and channel-open probability by influencing K^+ occupancy at sites below and within the SF. In line with this notion, mutations in the SF that change filter ion occupancy at the S1 and S4 sites (*17*, *26*) and induce the activated "leak mode" in K_{2P} channels (*17*) also render them insensitive to BL-1249 (and various other activators discussed below; fig. S6, A to D).

The negatively charged moiety identified within BL-1249, PD-118057, and NS11021 is also found in a series of known activators of TREK-1 and TREK-2 K_{2P} channels [ML67-33 (*27*), tetrazole; DCPIB (*28*), carboxylate], hERG channels [PD-307243 (*29*), carboxylate; NS3623 (*30*), tetrazole], and BK_{Ca} channels [GoSlo-SR-5-6 (*31*), sulphonate], and its requirement for channel activation has been demonstrated for ML67-33 and GoSlo-SR-5-6 (*27*, *31*). Indeed, these compounds also share all the hallmark features of BL-1249 action, including polypharmacology [i.e., mutual activation of K_{2P}, BK_{Ca}, and hERG channels (Fig. 4, C and D), sensitivity to QA_L^+ (Fig. 4A; fig. S7, A to C; and tables S2 and S3] and mutations that reduce BL-1249 activation in TREK-1 (fig. S4, C and D). In addition, MD simulations of their interaction with structures of the TREK-2, BK_{Ca}, and hERG channel pores identified similar stable binding poses below the SF with orientation of the negative moiety toward the cavity and a concomitant increase in K^+ occupancy at cavity and SF ion binding sites (Fig. 4, C and D, and figs. S7D and S8, A to C). Notably, this assumed NCA binding site overlaps with the "promiscuous inhibitor binding site" in the hERG channel, which underlies drug-induced long QT syndrome (*12*, *32*). This site is thought to accommodate many hydrophobic molecules (e.g., terfenadine), and consistent with this, we found that activation by PD-118057 strongly reduced inhibition by terfenadine (Fig. 4B).

The molecular features of the NCA compounds define a common pharmacophore that, besides the negatively charged group, comprises both aromatic and hydrophobic moieties (Fig. 4E). As a control, we tested tetrazole-containing compounds that do not fit this common pharmacophore on TREK-1, BK_{Ca}, and hERG channels and found that they were unable to promote channel activation (fig. S9, A to C).

Our results uncover a class of K^+ channel openers, the NCAs, that act as a universal master key to unlock the SF gate. Mechanistically, these NCAs bind below the SF, where their negative charge promotes K^+ binding to the pore cavity, and thereby also alter the ion occupancy in the SF in a way that is known to promote activation of the filter gate (*17*). We hypothesize that, in particular, the increase at the S1 and S4 sites is responsible for activating the SF gate because all NCA-responsive channels are also activated by Rb^+ permeation, which is thought to increase ion occupancy at these sites, whereas mutations known to reduce S1 and S4 ion occupancy in K_{2P} channels abolish NCA activation. Furthermore, a loss of K^+ binding to the S1 site has been implicated in SF inactivation in K_v channels (*33*), hERG channels (*32*), and TREK-2 K_{2P} channels (*19*). However, at this time, we cannot exclude the possibility that nonelectrostatic interactions of the NCAs with their respective binding sites also contribute to the stabilization of the active SF state because these sites involve gating-sensitive regions [i.e., the TM4 (*8*, *19*) and S6 segments (*6*, *34*)]. In any case, our results support the view that many K_{2P} channels, as well as BK_{Ca} channels, adopt a low-activity (i.e., inactivated) state of their SF at rest and that the various physiological stimuli induce structural changes that drive the SF into an active (open) state. The NCAs appear to operate by means of bypassing these activation mechanisms to directly stabilize the SF in its active state.

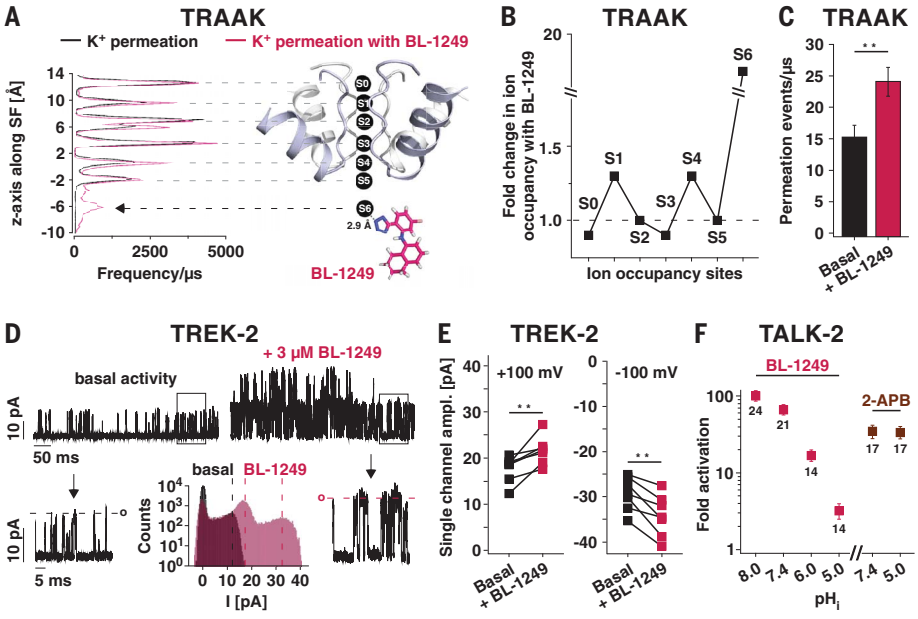

Fig. 3. Effects of BL-1249 on pore K^+ occupancy and permeation. (**A**) Ion occupancy (frequency/μs) of K^+ binding sites (S0 to S6) obtained from permeation MD simulations of TRAAK in the presence or absence of BL-1249, with BL-1249 adopting the identical position in TREK-2 (see Fig. 2G), that is, the negatively charged tetrazole ring (blue) in close proximity to the S6 K^+ ion. Coordinates were saved every 40 ps. The black arrow points to the increase in S6 K^+ occupancy. (**B**) Fold change in ion occupancy for the S0 to S6 sites. (**C**) MD simulations of K^+ permeation in TRAAK. Bars represent permeation events/μs from independent 200-ns MD simulations without (n = 50) and with BL-1249 (n = 30). $^{**}P \leq 0.01$. (**D**) Single-channel TREK-2 currents recorded at +80 mV from i-o patches before (basal) and after addition of 3 μM BL-1249, with arrows pointing to expanded scales of framed sections. The lower-middle panel depicts current amplitude histograms with or without 3 μM BL-1249 from i-o patches with ≤2 active channels (the right-hand peak represents the amplitude of two BL-1249–activated channels). Dotted lines indicate the single-channel amplitude maxima with or without BL-1249. (**E**) Paired single-channel current amplitudes before and after addition of 3 μM BL-1249 (n = 7). $^{**}P \leq 0.01$. (**F**) Fold activation of TALK-2 currents in i-o patches with 50 μM BL-1249 or 1 mM 2-APB applied at the indicated pH_i values. Error bars indicate SEM.

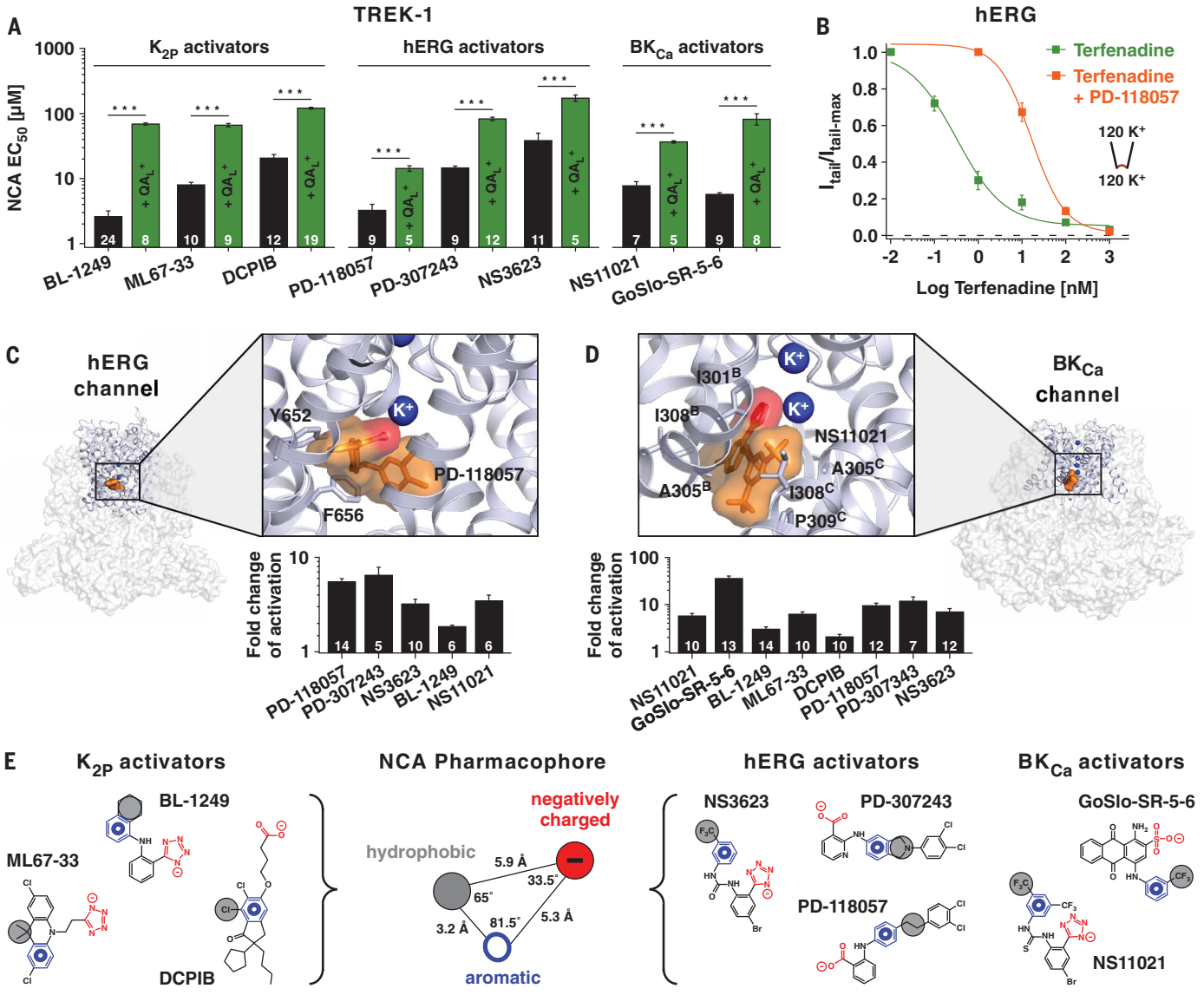

Fig. 4. NCA binding sites and common pharmacophores. (**A**) EC_{50} values (at +40 mV) for TREK-1 activation with compounds described as activators of either K_{2P}, hERG, or BK_{Ca} channels. Competitive antagonism is seen in the presence of QA_L^+ (either THexA or TPenA, which produce ~70 to 80% inhibition of respective basal K^+ currents). ***$P \leq 0.001$; error bars indicate SEM. (**B**) Terfenadine inhibition of hERG channels with or without 10 μM PD-118057. Error bars indicate SEM. (**C**) Structure of the hERG channel (PDB 5VA1) with the pore region expanded. This region was used for molecular docking and MD simulations to obtain the favored binding pose of PD-118057 (orange). Terfenadine-interacting residues are highlighted. The carboxylate group (red) interacts with a K^+ ion below the SF (see also fig. S7D); the bar chart below represents the fold activation of hERG tail currents at −100 mV with 10 μM of the indicated compounds. Error bars indicate SEM. (**D**) Same as in (C) but for the BK_{Ca} channel (PDB 5TJI), showing the favored binding pose of NS11021 (orange) where the tetrazole group (red) interacts with a K^+ ion below the SF and the residues in proximity to NS11021 highlighted. The bar chart below shows the fold activation of BK_{Ca} at +100 mV with 10 μM of the indicated compounds (at zero Ca^{2+}). Error bars indicate SEM; the B and C superscripts indicate the subunit of the tetramer. (**E**) Representation of the K_{2P}, hERG, and BK_{Ca} activators used to generate a common NCA pharmacophore consisting of aromatic (blue), hydrophobic (gray), and acidic (red) moieties, with distances and angles as shown.

In addition, our findings have important implications for the development of drugs that target K^+ channels, because they reveal the binding sites and the mechanism of action for many established activators in various K^+ channels. Our findings have also identified the first activators for several K_{2P} channels (e.g., TALK-1/-2 and THIK-1/-2). Notably, the NCA binding site overlaps with the promiscuous inhibitor site in hERG, and thus, targeting this NCA site might represent a promising approach to circumvent the drug-induced long QT syndrome, which is, as of now, a serious burden in drug development (*12*). However, the identified polypharmacology also represents a challenge for the development of any NCA-based compound into a highly subtype-specific K^+ channel agonist. Nevertheless, structural differences between K_{2P}, hERG, and BK_{Ca} channels may still permit a rational drug design that reduces this promiscuity. However, in some acute situations such as ischemic stroke or status epilepticus, exploiting the polypharmacology of NCAs to promote simultaneous opening of multiple neuroprotective K^+ channels (e.g., BK_{Ca}, TREK-1, TREK-2, TRAAK, THIK-1, and THIK-2) may even be beneficial.

REFERENCES AND NOTES

1. S. I. V. Judge, P. J. Smith, P. E. Stewart, C. T. Bever Jr., *Recent Pat. CNS Drug Discov.* **2**, 200–228 (2007).

2. V. K. Vyas, P. Parikh, J. Ramani, M. Ghate, *Curr. Med. Chem.* 10.2174/0929867325666180430152023 (2018).
3. S. Hou, S. H. Heinemann, T. Hoshi, *Physiology* **24**, 26–35 (2009).
4. M. I. Niemeyer, L. P. Cid, W. González, F. V. Sepúlveda, *Mol. Pharmacol.* **90**, 309–317 (2016).
5. F. V. Sepúlveda, L. Pablo Cid, J. Teulon, M. I. Niemeyer, *Physiol. Rev.* **95**, 179–217 (2015).
6. G. Yellen, *Nature* **419**, 35–42 (2002).
7. P. L. Piechotta *et al*., *EMBO J.* **30**, 3607–3619 (2011).
8. S. N. Bagriantsev, R. Peyronnet, K. A. Clark, E. Honoré, D. L. Minor Jr., *EMBO J.* **30**, 3594–3606 (2011).
9. C. M. Wilkens, R. W. Aldrich, *J. Gen. Physiol.* **128**, 347–364 (2006).
10. Y. Zhou, X.-M. Xia, C. J. Lingle, *Proc. Natl. Acad. Sci. U.S.A.* **108**, 12161–12166 (2011).
11. P. L. Smith, T. Baukrowitz, G. Yellen, *Nature* **379**, 833–836 (1996).
12. J. I. Vandenberg, E. Perozo, T. W. Allen, *Trends Pharmacol. Sci.* **38**, 899–907 (2017).
13. L. Pope *et al*., *ACS Chem. Neurosci.* **9**, 3153–3165 (2018).
14. J. Zhou *et al*., *Mol. Pharmacol.* **68**, 876–884 (2005).
15. B. H. Bentzen *et al*., *Mol. Pharmacol.* **72**, 1033–1044 (2007).
16. M. J. Lenaeus, D. Burdette, T. Wagner, P. J. Focia, A. Gross, *Biochemistry* **53**, 5365–5373 (2014).
17. M. Schewe *et al*., *Cell* **164**, 937–949 (2016).
18. J. G. McCoy, C. M. Nimigean, *Biochim. Biophys. Acta* **1818**, 272–285 (2012).
19. Y. Y. Dong *et al*., *Science* **347**, 1256–1259 (2015).
20. M. Rapedius *et al*., *Channels* **6**, 473–478 (2012).
21. R.-G. Zhuo *et al*., *Front. Cell. Neurosci.* **10**, 127 (2016).
22. M. Lolicato *et al*., *Nature* **547**, 364–368 (2017).
23. W. Kopec *et al*., *Nat. Chem.* **10**, 813–820 (2018).
24. M. V. Clausen, V. Jarerattanachat, E. P. Carpenter, M. S. P. Sansom, S. J. Tucker, *Proc. Natl. Acad. Sci. U.S.A.* **114**, E8343–E8351 (2017).
25. D. Kang, C. Choe, D. Kim, *J. Physiol.* **564**, 103–116 (2005).
26. M. Zhou, R. MacKinnon, *J. Mol. Biol.* **338**, 839–846 (2004).
27. S. N. Bagriantsev *et al*., *ACS Chem. Biol.* **8**, 1841–1851 (2013).
28. L. Minieri *et al*., *Br. J. Pharmacol.* **168**, 1240–1254 (2013).
29. E. Gordon *et al*., *Mol. Pharmacol.* **73**, 639–651 (2008).
30. R. S. Hansen *et al*., *Mol. Pharmacol.* **70**, 1319–1329 (2006).
31. S. Roy *et al*., *ChemMedChem* **7**, 1763–1769 (2012).
32. W. Wang, R. MacKinnon, *Cell* **169**, 422–430.e10 (2017).
33. V. Pau, Y. Zhou, Y. Ramu, Y. Xu, Z. Lu, *Nat. Struct. Mol. Biol.* **24**, 857–865 (2017).
34. H. Yang, G. Zhang, J. Cui, *Front. Physiol.* **6**, 29 (2015).

ACKNOWLEDGMENTS

We thank F. Lesage for the THIK-1 and THIK-2 K_{2P} channel clones; M. A. Hollywood for providing the BK_{Ca} activator GoSlo-SR-5-6; and J. Kusch for initially testing the BL-1249 effect on CNGA1 channels. We thank all members of our respective laboratories for technical support and comments on the manuscript. We thank Diamond Light Source Ltd. and its staff for access to the macromolecular crystallography beamlines. We also acknowledge the North-German Supercomputing Alliance (HLRN) for providing High Performance Computing (HPC) resources that have contributed to the research results reported in this paper. **Funding:** T.B. and B.L.d.G. were supported by the DFG; B.F. was supported by the DFG (SFB746, TRR 152, and EXC 294 and 2189); S.J.T. and E.P.C were supported by a BBSRC Industrial Partnership Award (BB/N009274/1); and L.J.C. was supported by a Wellcome Trust (OXION) Ph.D. studentship. A.M. was funded by the EPSRC Life Sciences Interface Doctoral Training Centre. A.C.W.P. and E.P.C. are members of the SGC (charity reference no. 1097737) funded by AbbVie, Bayer Pharma AG, Boehringer Ingelheim, the Canada Foundation for Innovation, Genome Canada, Janssen, Merck KGaA, MSD, Novartis, the Ontario Ministry of Economic Development and Innovation, Pfizer, São Paulo Research Foundation-FAPESP, and Takeda, as well as the Innovative Medicines Initiative Joint Undertaking ULTRA-DD grant 115766 and the Wellcome Trust 106169/Z/14/Z. D.C.P. was an employee of Pfizer at the time of the research. **Author contributions:** M.S. and T.B. conceived the study and designed the electrophysiological experiments. M.S., Ü.M., F.S., and M.T. performed all inside-out patch-clamp experiments in *Xenopus* oocytes. M.S. and T.B. analyzed the data. M.M. designed K^+ channel mutations. C.C. performed whole-cell recordings in CHO cells and analyzed the data together with B.F. Single-channel recordings in *Xenopus* oocytes were carried out and analyzed by K.S.V. and A.K.K., supervised by N.D. Single-channel recordings in HEK293 cells were performed and analyzed by L.J.C., supervised by S.J.T. A.M. purified TREK-2 and cocrystallized TREK-2 with BL-1249$^{Br.}$. A.M. and A.C.W.P. obtained and analyzed the x-ray data, supervised by E.P.C. and S.J.T. D.C.P. synthesized the brominated BL-1249. H.B. synthesized ML67-33, supervised by M.N. H.S. designed, performed, and analyzed all molecular dockings and MD simulations with critical comments of B.L.d.G. W.G. calculated and analyzed the NCA pharmacophore together with M.S. and N.D. M.S. and M.M. prepared and edited all figures. T.B., M.S., B.F., E.P.C., and S.J.T. contributed to the writing and editing of the manuscript and approved the manuscript. **Competing interests:** The authors declare no competing interests. **Data and materials availability:** All data are available in the main text or the supplementary materials. Requests for materials should be addressed to the corresponding authors.

SUPPLEMENTARY MATERIALS

www.sciencemag.org/content/363/6429/875/suppl/DC1
Materials and Methods
Figs. S1 to S9
Tables S1 to S3
References (*35*–*67*)

9 August 2018; accepted 28 January 2019
10.1126/science.aav0569

A pharmacological master key mechanism that unlocks the selectivity filter gate in K^+ channels

Marcus Schewe, Han Sun, Ümit Mert, Alexandra Mackenzie, Ashley C. W. Pike, Friederike Schulz, Cristina Constantin, Kirsty S. Vowinkel, Linus J. Conrad, Aytug K. Kiper, Wendy Gonzalez, Marianne Musinszki, Marie Tegtmeier, David C. Pryde, Hassane Belabed, Marc Nazare, Bert L. de Groot, Niels Decher, Bernd Fakler, Elisabeth P. Carpenter, Stephen J. Tucker and Thomas Baukrowitz

Science **363** (6429), 875-880.
DOI: 10.1126/science.aav0569

A key to potassium channel activation

Using drugs to activate potassium channels has the potential to treat conditions like epilepsy, heart arrhythmias, and pain. Schewe *et al.* report a class of negatively charged activators (NCAs) with a defined pharmacore that use a similar mechanism to activate many types of potassium channels. X-ray crystallography, functional analysis, and molecular dynamics simulations showed that the NCAs bind below the selectivity filter to open the filter gate and activate the channels. Targeting this NCA site might be exploited in rational drug design.

Science, this issue p. 875